Space Weather Effects on the Ionosphere:

Alan Wood (alan.wood@ntu.ac.uk), Nottingham Trent University

The Mid-Latitude Ionosphere

Plasma Production by Photoionisation

$$q = C \cdot n \cdot \sigma \cdot I$$

q is the ion production rate (in s^{-1})
C is the ionisation efficiency (approx. 1 ion pair per 35 eV lost)
n is the number density of the neutral atmosphere (in m^{-3})
σ is the scattering cross section (in m^2)
I is the intensity of the incoming radiation (in eV m^{-2} s^{-1})

n decreases exponentially with increasing altitude
I decreases exponentially as sunlight enters the atmosphere
Some location where production maximises
Around 250 km; even at the peak only ~1% of the atmosphere is ionised
Varies with solar cycle

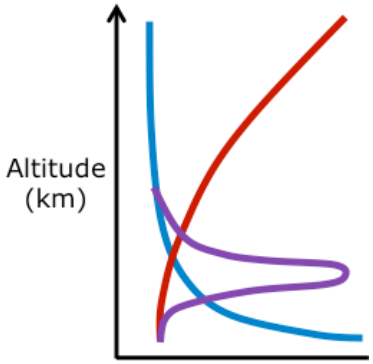

Assumptions:

- Atmosphere is comprised of a single species, exponentially distributed with altitude
- Plane stratified atmosphere
- Absorption co-efficient is constant

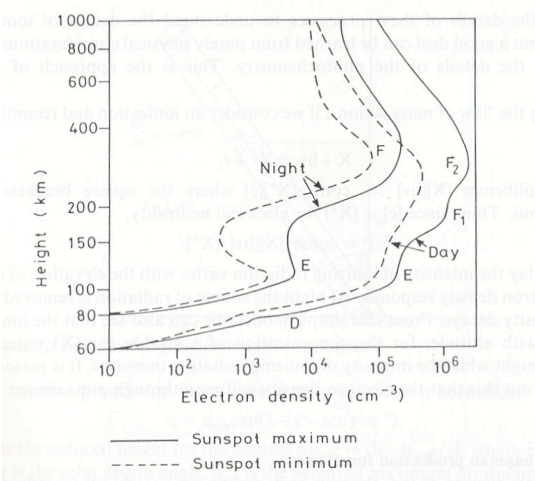

Image Credit: Hargreaves, (1997) after W. Swider, Wallchart, Aerospace Environment, US Air Force Geophysics Laboratory.

Chapman Production Function

Production varies during the day

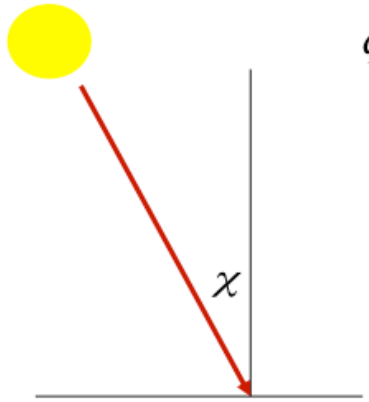

$$q = C \cdot n \cdot \sigma \cdot I$$

$$q = q_{m0} \cdot \exp\left(1 - z - \sec\chi \cdot e^{-z}\right)$$

$$z = \frac{h - h_{m0}}{H}$$

z is the reduced height, h is height, H is scale height, χ is the solar zenith angle, q_{m0} is the production rate at h_{m0} when the sun is overhead

Loss by recombination with the neutral atmosphere

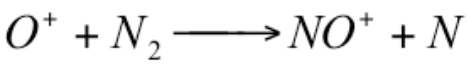

Rearrangement

Dissociation

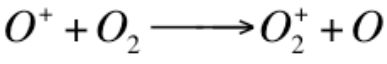

Rearrangement

Dissociation

In both cases it is the rearrangement reaction which dominates

$$\delta N_e = k_1 [N_2][N_e] + k_2 [O_2][N_e]$$

N_e is the plasma density (in m^{-3})

δN_e is the change plasma density (in $m^{-3}\,s^{-1}$)

$[N_2]$ is the number density of N_2 (in m^{-3})

$[O_2]$ is the number density of O_2 (in m^{-3})

k_1 and k_2 are reaction rates (in $m^3\,s^{-1}$)

Day to night

Electron temperature falls.

Electron density falls as plasma decays due to chemical reactions with the atmosphere.

$$\delta N_e = \left(k_1 [N_2]\right) N_e$$

Electron density falls faster at lower altitudes. So the altitude of the peak electron density increases.

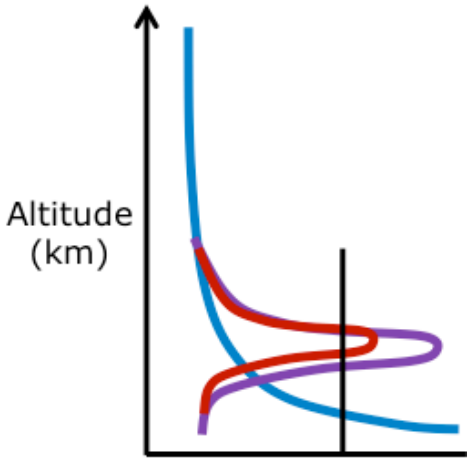

Ionosondes

Transmit at a range of frequencies

The refractive index of the ionosphere is proportional to the electron concentration and inversely proportional to the frequency of the wave

Different frequencies reflected at different altitudes; gives information on the structure and density of the ionosphere

Chilton Ionosonde: Data goes back to 1931

UKSSDC

Click on "World Data Centre for Solar-Terrestrial Physics"

"Ionospheric"

"Prompt Data" (not "Ionosphere Data Catalogue")

"Go to the database"

Other useful data (such as Kp, F10.7cm Solar Flux) in "World Data Centre for Solar-Terrestrial Physics", "Geophysical"

Anomalies

Seasonal Anomaly: Electron densities are greater in winter, due to changes in the chemical composition of the atmosphere. Upwelling in summer makes the atmosphere more molecular at a given altitude

Plasma production depends on the number density of atomic oxygen

Plasma loss depends on the the number density of molecular species

Semiannual anomaly: Global electron density is larger at the equniox than at solstice. At solstice a greater temperature gradient between poles, drives a summer-to-winter flow transporting molecular rich air

Annual Anomaly: The global averaged plasma density is greater in December than in June. Sun-Earth distance varies. Resulting EUV incident on the Earth varies by 6%. Variation observed is ~20%

Prediction of bulk properties: A non-trivial task, some successes, i.e. Ünal et al. (2011) used neutral networks to predict foF2

Structures at Mid Latitudes: Travelling Ionospheric Disturbances (TIDs)

Gravity waves cause oscillations in the neutral atmosphere

These can be communicated to the ionised atmosphere through collisions and cause TIDs

- Small scale (λ ~ 150 km): Severe weather in troposphere
- Medium scale (λ ~ 300 km): Thunderstorms? Jet streams?
- Large scale (λ > 1000 km): Auroral activity?

Typical variation in plasma density of ~ 1%. Can be up to ~ 5%.

The Low Latitude Ionosphere

Plasma production by photoionisation

Plasma loss through reactions with the neutral atmosphere

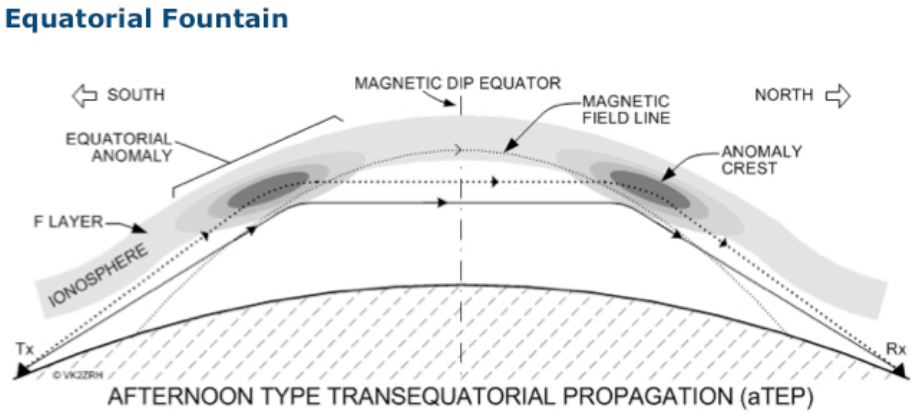

Image Credit: Roger Harrison

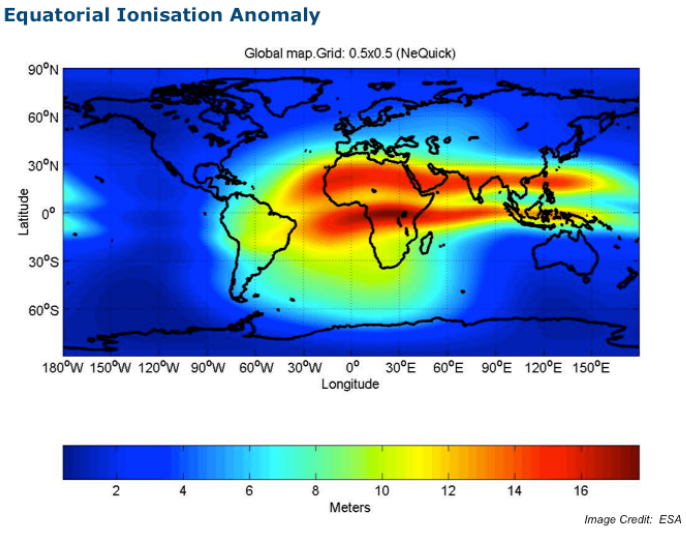

Image Credit: ESA

Space Weather Effects

Plasma Structures: Disruption to trans-ionospheric radio signals

Global Navigation Satellite Systems (GNSS)

Examples include GPS, Galileo & Glonass

GNSS satellites are effectively atomic clocks in orbit, broadcasting a code giving the time and their position

If a device can 'see' at least four of these satellites and measure the time between transmission and reception of the code, can get the position to +/- 5 m

Higher precision: Track the carrier wave. Two frequencies; go out of phase in proportion to the electron density. With a sufficiently large number of satellites the position error can be reduced to 1mm

The electron density in the ionosphere varies throughout the day

Also get positioning and timing errors due to plasma structures

These structures can also cause loss of lock

Satellite Based Augmentation System (SBAS For aircraft navigation)

Data from numerous stations allow a grid to be formed (say 5^{o} x 5^{o}) giving the ionospheric correction at each point

At equator plasma bubbles can give an error of 850 mm / km

The Aurora: Historical Observations

30,000 BC:	Cave paintings, France
2,600 BC:	Possibly mentioned in Chinese writings
450 BC:	Observed in Greece
1230 AD:	The King's Mirror, Norway
1400s:	Noticed that compasses did not point to true north.
1635:	Saw that this changed with time *(Gellibrand, London).*
1724:	Saw that variations in the magnetic field were associated with the northern lights (Graham, London).
1750:	See variations in the magnetic field, predicted aurora (Wargentin, Sweden).

The Aurora

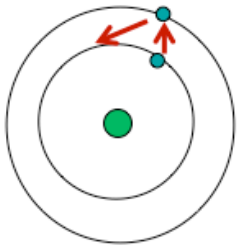

The colour of the aurora

$$E = \frac{h \cdot c}{\lambda}$$

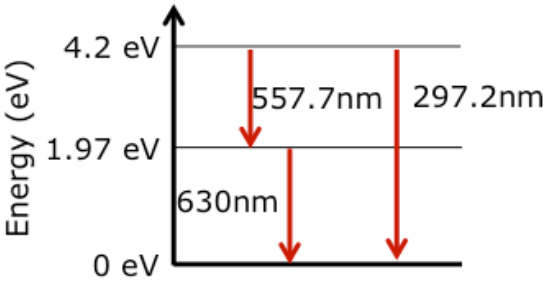

What we observe also depends upon the sensitivity of our eyes, the lifetime of the excited state and the energy of the precipitating particles

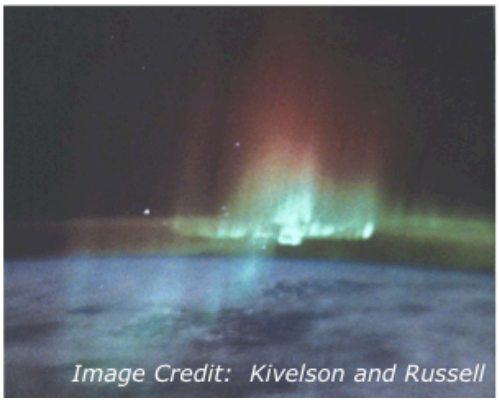

Plasma Production and Transportation

Plasma Production

Photoionisation (sunlight)

Precipitation (northern lights)

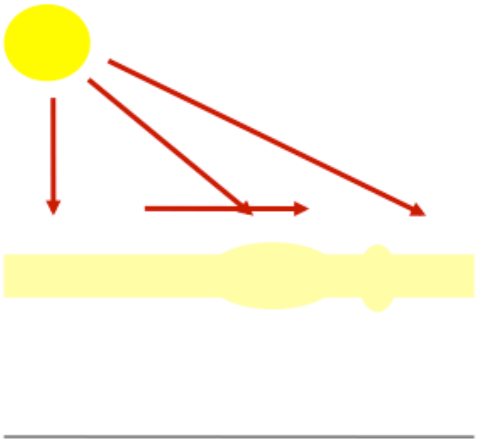

Transportation

Occurs due to the interaction of the Earth's magnetic field and the magnetic field carried by the solar wind

Can move and create structures

Magnetic Reconnection

In a low density plasma, such as that in the solar wind, there is a very low chance of any collisions.

So particles spiral along field lines; frozen to the magnetic field.

But get places with large gradients in B over short spatial scales. Then frozen in condition no longer applies.

Magnetic reconnection is a process which happens when the frozen in condition breaks down.

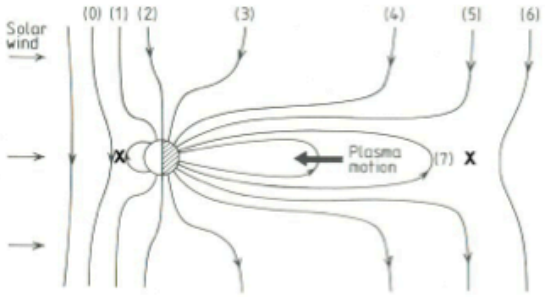

Image Credit: Brekke (1997)

Magnetic Reconnection

Magnetic field lines "break" and "reconnect", releasing magnetic energy and accelerating some particles.

Magnetic reconnection directly affects very few particles. It is the reconfiguration of the magnetic field that affects most.

Div B = 0 is not violated. If draw a sphere, still the same 'number' of field lines in and out, just a different configuration.

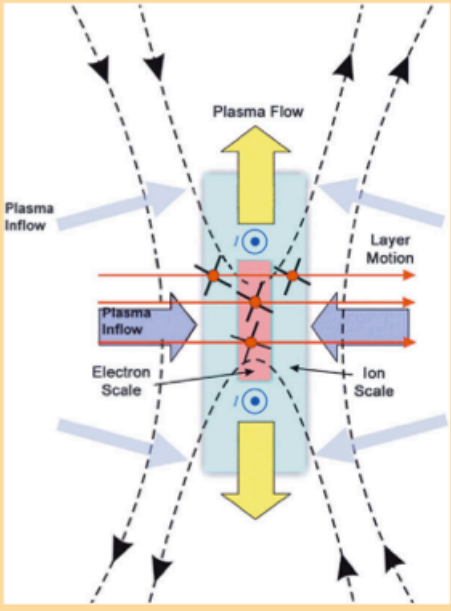

Figure 1. *This figure shows the classic reconnection scenario at an X line. The black dashed lines are field lines. The thick purple and yellow arrows indicate plasma flow into and out of the reconnection region. The pink and green regions show the diffusion regions of the electrons and ions, respectively. The strong current out of the page (blue arrow heads) is consistent with the strong curvature of the magnetic field in the outflow region. The black crosses with red dots represent the four MMS spacecraft in the ideal position to observe reconnection as the reconnection regions moves over them (thin red arrows). (Modified from http://mms.space.swri.edu/mission-3.html.)*

The weak B field near the centre of the current sheet lets the E field accelerate particles.

Particle models look at the behaviour of individual particles; fluid models look at the behaviour of ensembles of particles based on the statistical properties of that ensemble.

Often treat reconnection as black box. Don't yet know how fast reconnection is and why.

Electric and Magnetic Field

The magnitude of a force that an electric field and a magnetic field B exerts on a charged particle is:

$$F = q \cdot E + q \cdot v \times B$$

E x B drift

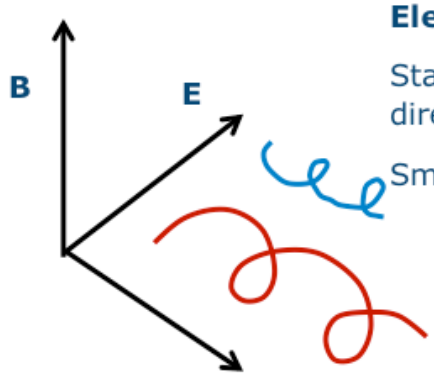

Electron

Starts to move in the opposite direction

Smaller radius

$$r_c = \frac{m \cdot v}{q \cdot B}$$

Plasma Transportation

Solar wind gives rise to an electric field

$$F = q \cdot E + q \cdot v \times B$$

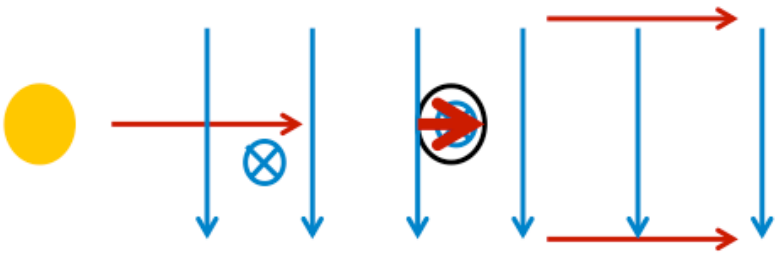

Drives ionospheric plasma from day to night across the pole for IMF B_z negative or when IMF B_y dominates

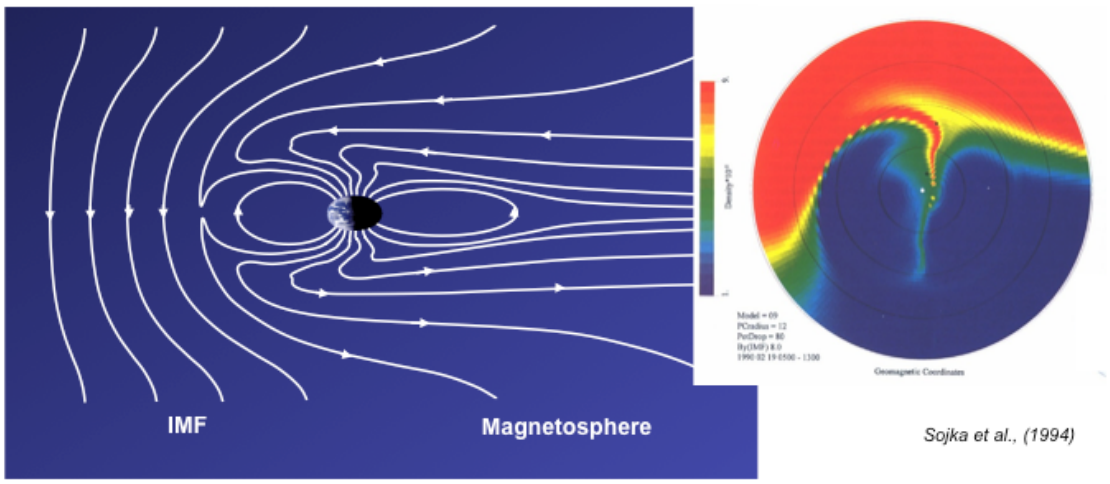

Drives ionospheric plasma from day to night across the pole for IMF B_z negative or when IMF B_y dominates

Variation in IMF B_y displaces the cross polar antisunward flow towards dawn (dusk) for positive (negative) values in the northern hemisphere

Patches

Variations in the transport process break this plasma into a series of discrete polar cap patches

Buchau et al. (1983) observed patches of enhanced ionisation in the central region of the polar cap at Thule, Greenland

Weber et al., (1986) observed an individual patch for over 3000 km

Defined by Crowley (1996) as having a plasma density of at least twice the surrounding background value and a minimum horizontal spatial extent of 100 km

Numerous formation mechanisms, for example:

- Transient bursts of reconnection *(Lockwood and Carlson, 1992)*
- Variation in IMF B_y *(Sojka et al., 1993)*
- Variation in IMF B_z *(Valladares et al., 1998)*
- Flow channel event *(Rodger et al., 1994)*
- Modulation of plasma densities by precipitation *(Walker et al., 1999)*

Day to night transport

Electron temperature falls.

Electron density falls as plasma decays due to chemical reactions with the atmosphere.

Electron density falls faster at lower altitudes. So the altitude of the peak electron density increases.

Sporadic E

Plasma also moves due to collisions with the neutral atmosphere

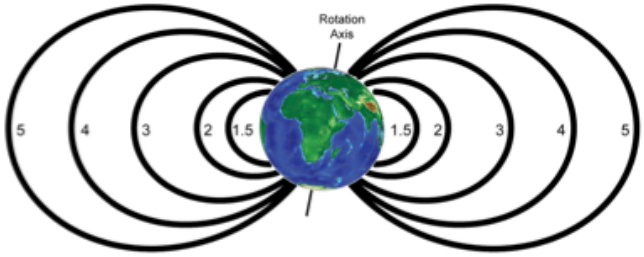

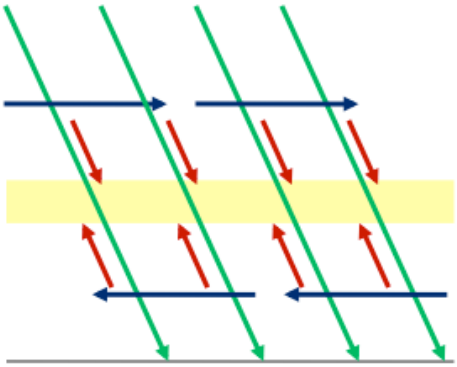

Auroral Oval

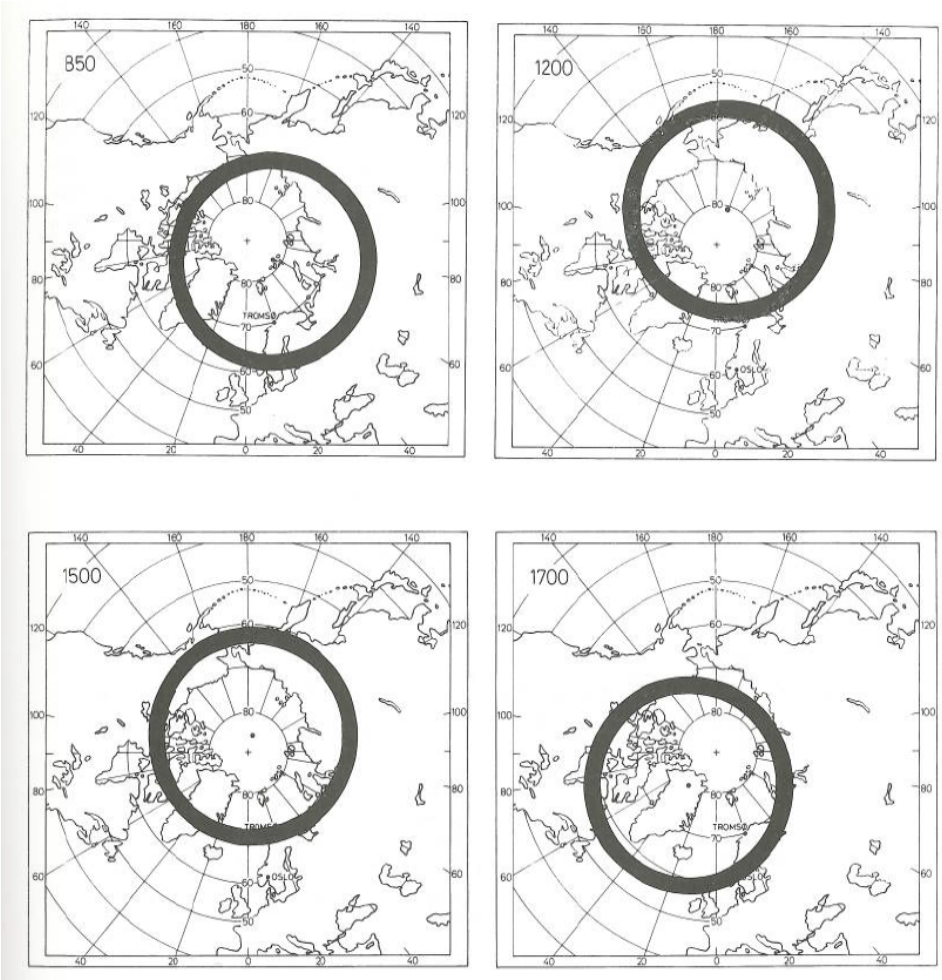

Image Credit: Brekke (1997)

The Aurora: Currents

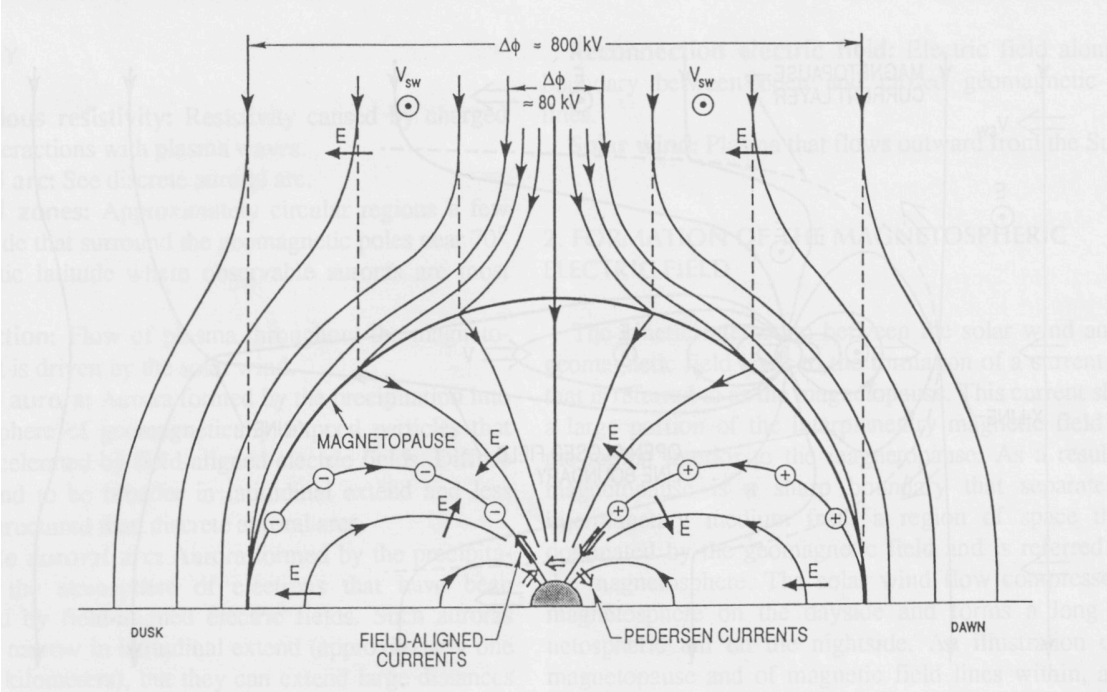

Image credit: Lyons (1992)

Antiparallel magentic field lines associated with a current. Flows westwards (duskwards) in the magnetotail.

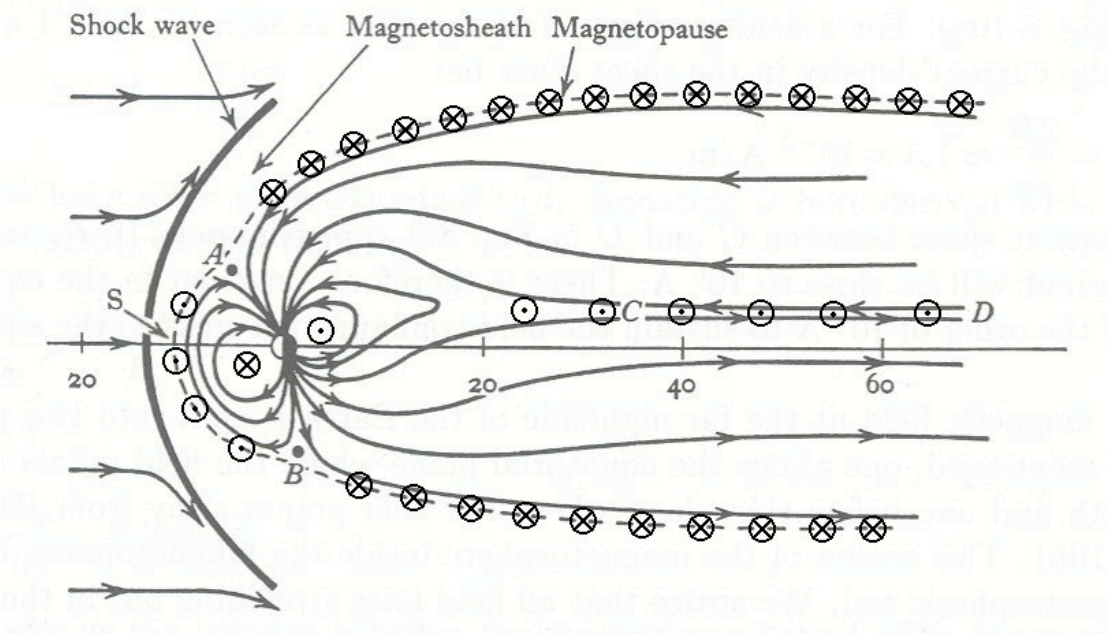

Image credit: Hess (1967)

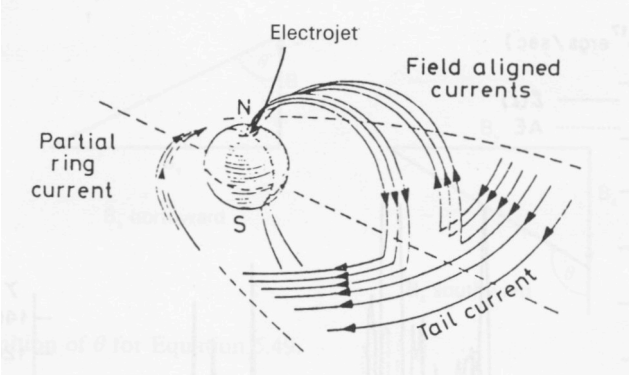

Image credit: Svalgaard (1975)

Plasma moves Earthward; conductivity is enhanced on field lines

Cross-tail current diverted

E-region conductivity is enhanced

Cross-tail current diverted

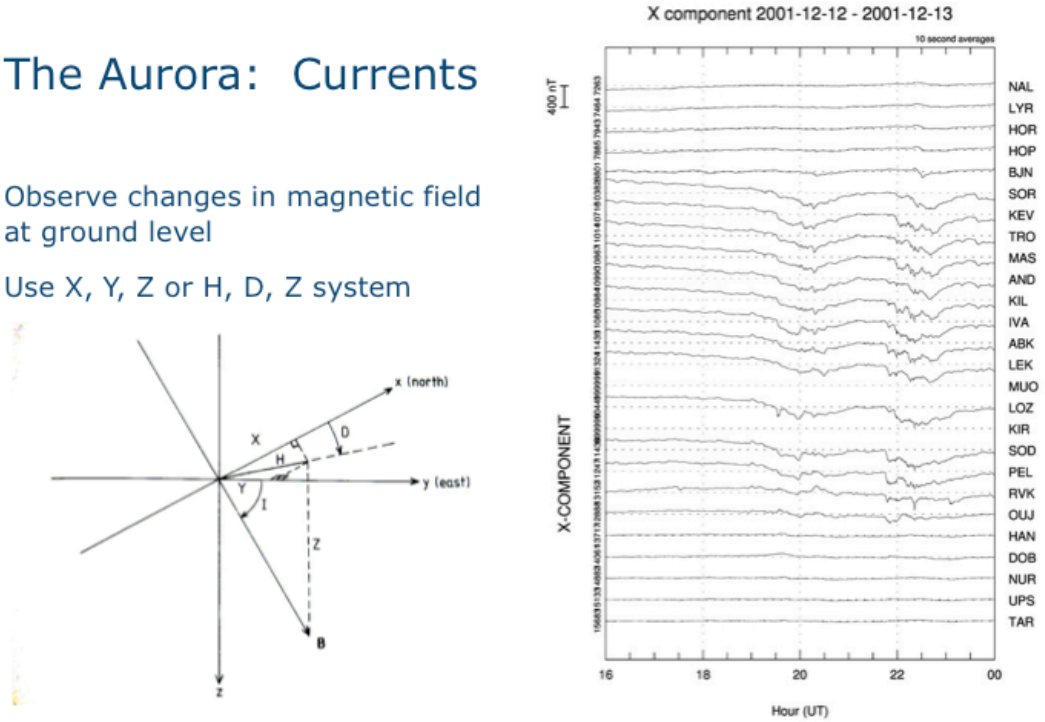

Look at variations from quiet conditions

Numerous auroral / high-latitude indices, for example AE (auroral electrojet index) and Kp (planetary K index) use different networks of magnetometers

Process depends upon the solar wind conditions; the bulk properties of the solar wind and the strength & orientation of the Interplanetary Magnetic Field

Auroral Substorm

Growth phase: IMF B_z becomes negative; magnetotail becomes stretched; polar cap expands

Expansion phase: Reconnection occurs; polar cap contracts, spectacular auroral displays move poleward

Recovery phase

Space Weather Effects

Geomagnetically Induced Currents (GICs)

Damage to power lines and transformers

For power grids it is dB/dt which is important. This was 1000 nT/min for the Quebec event (although it is thought that 435nT/min would have been enough to cause the failure)

500 nT/min gives 'recoverable problems' on the grid

Would want to know GIC 4-5 days in advance, as this is how long it takes to shut down the network in a controlled manner

Statnett (Norway) say they would want to know GIC 4-5 days in advance, as this is how long it takes to shut down the network in a controlled manner.

This kind of warning is not really possible. So:

- Set trip levels to protect transformers
- Build transformers that are more robust (but still can't deal with a Carrington event)
- Neutral line blocking system, but this is expensive and we don't know if it will work, so it is rarely done
- Neutral capacitor blocking device, but this is expensive and we don't know if it will work, so it is rarely done

Disrupt technological systems

Low Latitudes: Ring Current

Occurs as ions and electrons as approach the Earth

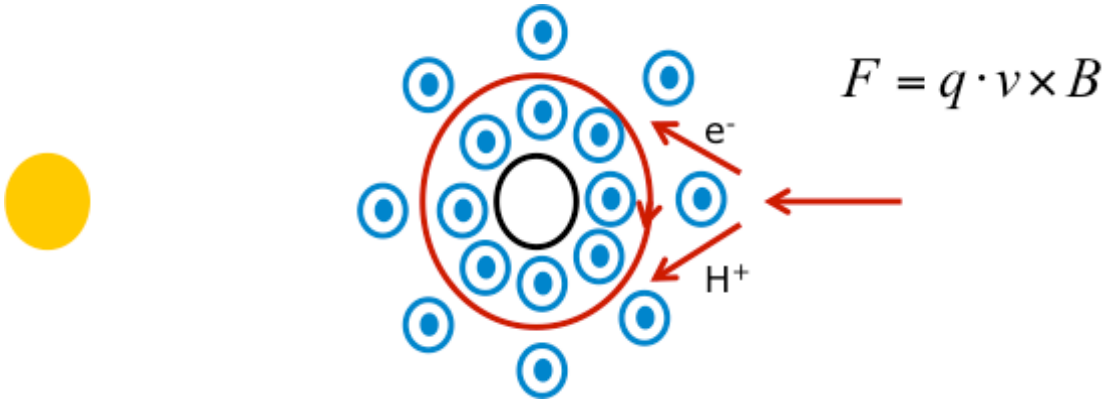

Magnetic reconnection gives rise to the ring current

Ring current causes disturbances to the Earth's magnetic field

A network of magnetometers produces the DST (Equatorial Disturbance Storm Time Index)

More negative, more disturbed

Multi-instrument case studies

For example:

- EISCAT: Time series at a point
- Ionospheric radiotomography: Spatial snapshot
- SuperDARN: Convection pattern

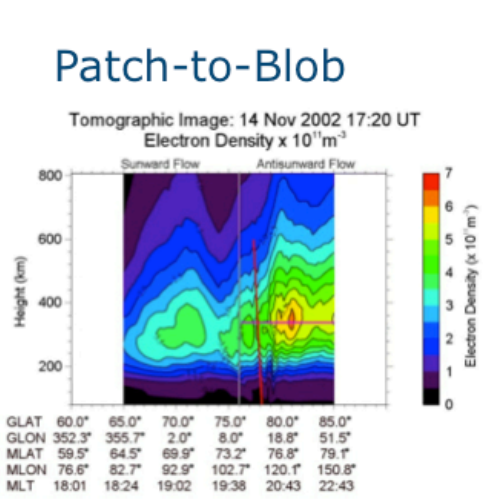

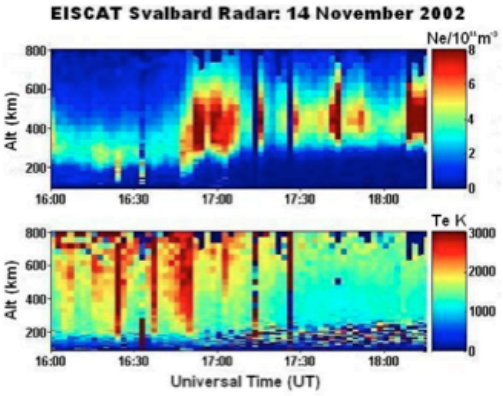

High altitude, low temperature

-> Plasma transport

Note different altitudes from EISCAT and tomography

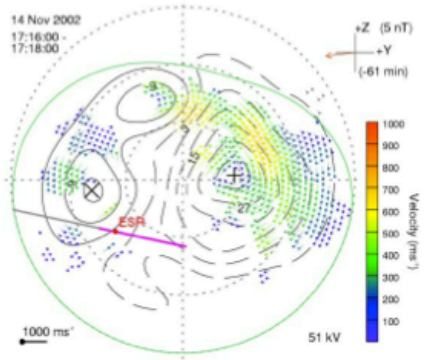

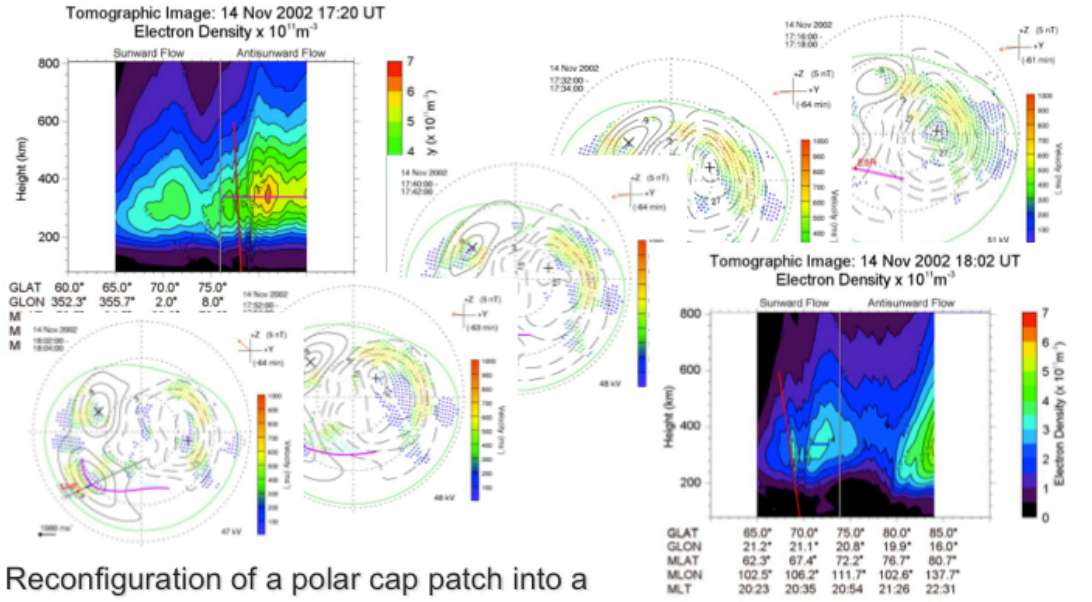

Reconfiguration of a polar cap patch into a boundary blob

Pryse et al., Ann. Geophys. (2006)

Plasma Transport Case Study

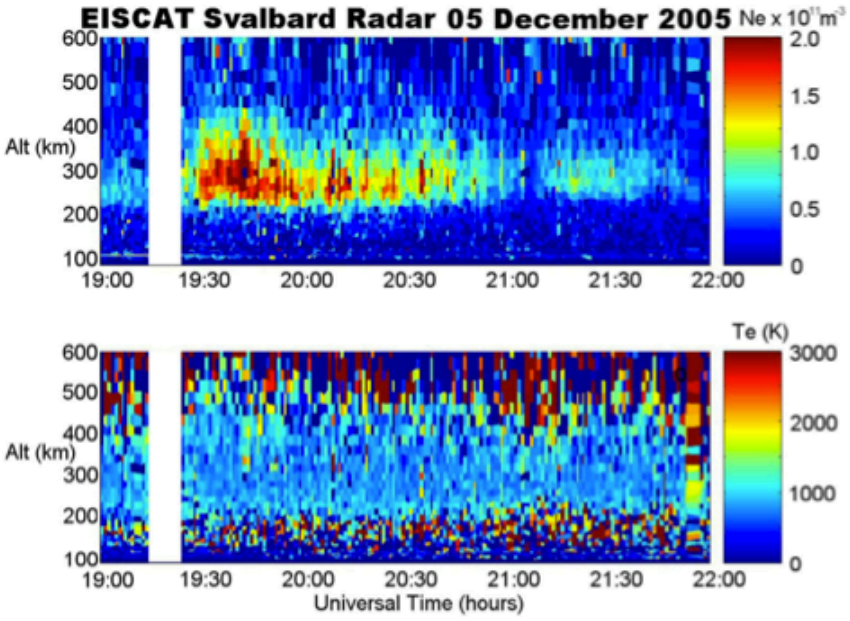

Fig. 2. Electron densities (top panel) and electron temperatures (bottom panel) measured by the 42 m dish of the EISCAT Svalbard Radar observing along the geomagnetic field between 19:00 UT and 22:00 UT on 5 December 2005.

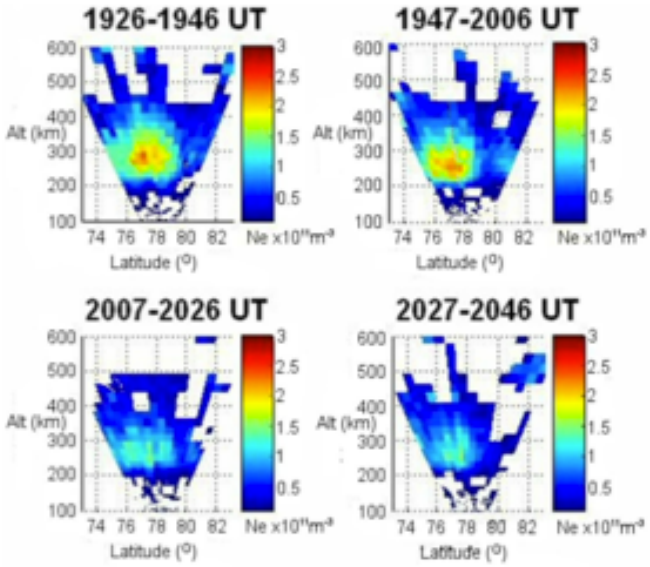

Fig. 3. Electron densities measured by the 32 m dish of the EISCAT Svalbard Radar scanning from north to south along the geographic meridian between 19:26 UT and 20:46 UT on 5 December 2005.

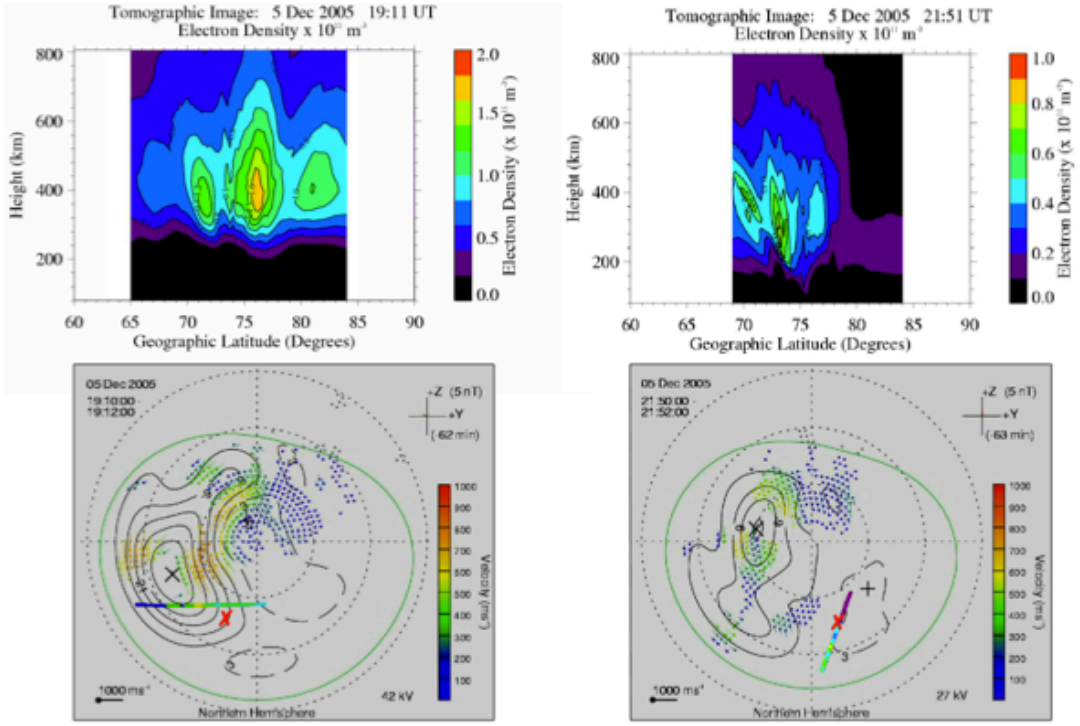

Fig. 4. Electron densities observed by the radio tomography experiment during a satellite pass that crossed a latitude of 75° N at 19:11 UT (top left panel) and 21:51 UT (top right panel), and the corresponding electric potential patterns inferred from the SuperDARN radars at 19:11 UT (bottom left panel) and 21:51 UT (bottom right panel). The multicoloured lines on the potential maps indicate the satellite trajectories intersecting the ionosphere at an altitude of 350 km with the colours representing the electron density at the F-region peak of the tomography image. To clearly show the electron density observed by the radio tomography experiment at 21:51 UT an electron density scale is used in the right hand panels with a maximum value of half that used in the left hand panels. The red crosses represent the position of the EISCAT Svalbard Radar.

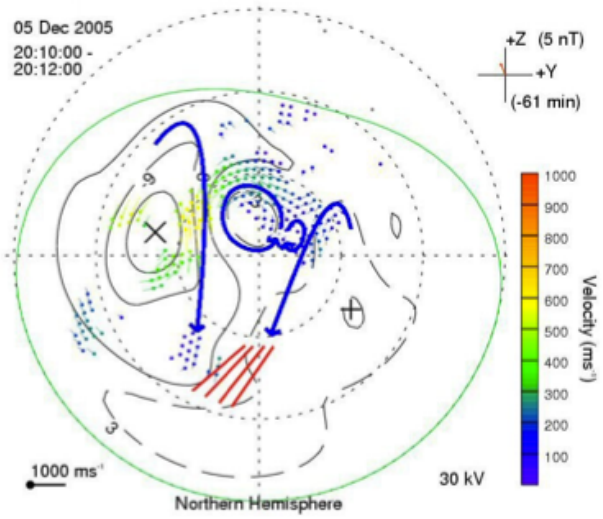

Fig. 6. Electric potential pattern inferred from the SuperDARN radars for 20:10 UT on 5 December 2005. The red lines indicate the positions of the 300 km ionospheric intersection of successive scans by the EISCAT Svalbard Radar commencing at 19:26 UT, 19:47 UT, 20:07 UT and 20:27 UT. The blue curves are a schematic of the high latitude convection pattern.

Wood et al., Ann. Geophys., 2008.

Space Weather Effects: Scintillation

Low latitudes: Amplitude scintillation dominates

High latitudes: Phase scintillation dominates

- A direct connection between gradients in the Total Electron Content (TEC) and scintillation has been observed (Mitchell et al., 2005)
- Plasma structuring caused by auroral precipitation has been linked to the loss of signal lock by a GNSS receiver (Elmas et al., 2011; Smith et al., 2008).
- Statistical studies have shown an agreement between scintillation and the asymmetric distribution of polar cap patches around magnetic midnight (Spogli et al., 2009) and that auroral emissions correlate with GNSS signal scintillation (Kinrade et al., 2013).

Polar Cap Patches in the High-Latitude Ionosphere in Northern Deep Winter: The Presence and Absence of Scintillation

Isobel Ching, Alan Wood and Luke Jenner

School of Science and Technology, Nottingham Trent University, Nottingham, United Kingdom (alan.wood@ntu.ac.uk)

NOTTINGHAM TRENT UNIVERSITY

Abstract

Two large-scale plasma structures were observed drifting antisunward on the evening of the 14th December 2015 under moderately disturbed conditions (Kp=5). One of these structures was associated with particle precipitation and scintillation of GNSS signals passing through this volume was observed. The other structure was identified as being a polar cap patch and it showed an absence of both particle precipitation and scintillation. This suggests that small-scale irregularities had not grown within this large-scale plasma structure as it was transported across the polar cap.

Background

The high-latitude ionosphere is a highly complex plasma containing electron density structures with a wide range of spatial scale sizes. Large-scale structures, such as polar cap patches, can also cause smaller-scale irregularities that arise due to instability processes. These smaller scale structures can disrupt trans-ionospheric radio signals, including those used by Global Navigation Satellite Systems (GNSS).

Electron Density and Temperature

Electron densities and temperatures were observed using the EISCAT Svalbard Radar (ESR, 78.2°N, 16.0°E) and the EISCAT VHF radar (69.6°N, 19.2°E). The 42m dish of the ESR was observing along the geomagnetic field line, the 32m dish was observing southwards at low elevation (30°) and the VHF radar was observing northwards at low elevation (30°).

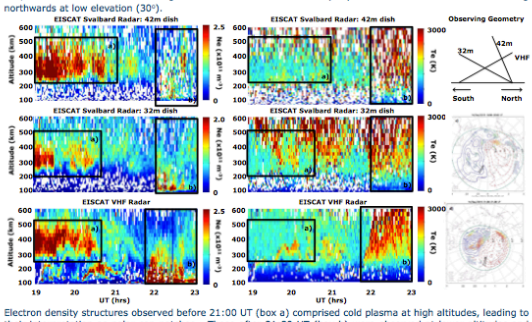

Electron density structures observed before 21:00 UT (box a) comprised cold plasma at high altitudes, leading to their interpretation as polar cap patches. Those after 21:30 UT (box b) were observed at lower altitudes and had a greater temperature, suggesting that they are due to particle precipitation. Comparison with SuperDARN plots (above right, the locations of the radar beams are shown as black lines) and EISCAT velocity measurements (not shown) suggest that the radars are located in a region of cross polar flow. The observing geometry of the radars (top right) shown that enhancements in cross-polar flow would be observed first by the 42m dish of the ESR, with the other radars observing these enhancements at a later time.

Polar Cap Patch Velocity

The velocity of the polar cap patch can be estimated from observations of airglow made using a Meridian Scanning Photometer (MSP) at Svalbard (below left), approximately co-located with the ESR. Box a shows the times when the ESR observed polar cap patches and box b shows times associated with particle precipitation. The 'S' shaped curves in box a result from polar cap patches drifting through the field of view of the instrument. The component of their velocity in the equatorward direction was typically ~130 m s^{-1}.

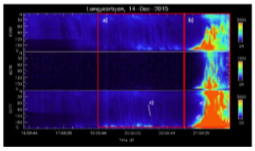

Phase Scintillation

Observations of phase scintillation were made using a scintillation receiver at Svalbard (right), owned by the University of Bergen. The bold text shows the peak phase scintillation value, while the italicised data is co-located with the ESR.

Time (UT)	Phase Scint. (rad)	Time (UT)	Phase Scint.
22:06	0.45	22:17	0.37
22:07	0.3	22:18	0.31
22:10	**0.71**	22:19	0.64
22:10	0.37	22:22	0.31
22:11	0.35	22:27	0.57
22:14	0.62	22:49	0.31
22:15	0.38	22:58	0.33

Phase Scintillation & Plasma Structures

The locations at which phase scintillation occurred can be compared to those of the plasma structures for times relating to the polar cap patches (1900-2030UT, lower left panel) and auroral precipitation (2200-2300 UT, lower right panel). The black lines show the pointing directions of the radars. The grey lines indicate satellite tracks with colours indicating scintillation. Scintillation is present when precipitation is observed, but is absent when polar cap patches are observed.

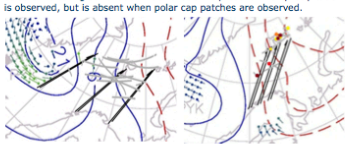

Discussion

Van der Meeren et al. (2015) observed severe phase scintillating in the nightside high-latitude ionosphere during a substorm, under moderately distributed conditions (Kp=2). In this study auroral scintillation was highly localised and that the strong scintillation did not extend into polar cap patches.

The present study, under more disturbed conditions, also shows a lack of phase scintillation in polar cap patches, suggesting that small-scale irregularities had not grown within these patches, even under these more disturbed conditions.

Reference: van der Meeren et al. (2015), Severe and localized GNSS scintillation at the poleward edge of the nightside auroral oval during intense substorm aurora, J. Geophys. Res.Space Physics,120, 10,607–10,621,doi:10.1002/2015JA021819

Acknowledgements: *EISCAT data were provided by the EISCAT Support Group at Rutherford Appleton Laboratory, phase scintillation data were provided by the University of Bergen, MSP data were provided by UNIS and SuperDARN data were obtained from vt.superdarn.org.*

Structuring Ratio

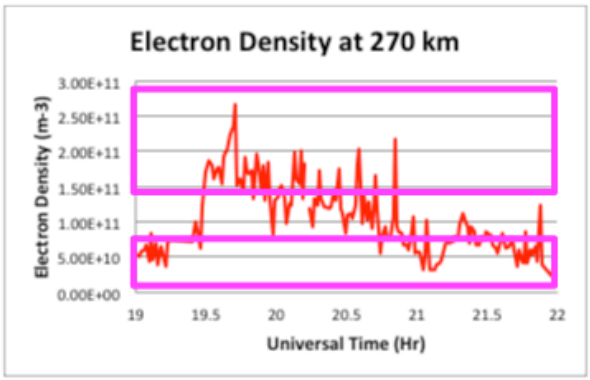

Larger Ne: 1.8×10^{11} m^{-3}

Smaller Ne: 0.5×10^{11} m^{-3}

Structuring Ratio: 3.6

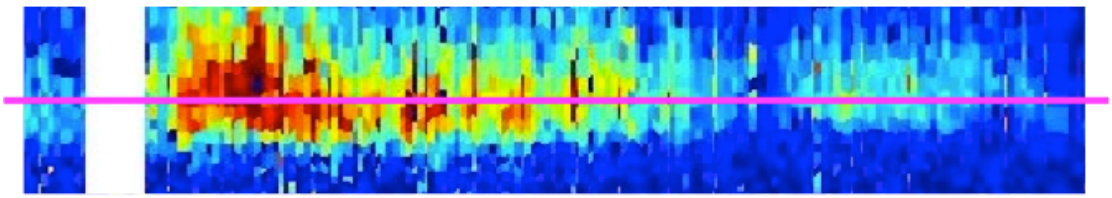

Peak Altitude: 270 km

EISCAT Svalbard Radar observations

- Around solar maximum
- IMF B_z predominantly negative
- ESR in antisunward cross polar flow
- ESR poleward of Harang discontinuity
- No evidence of precipitation

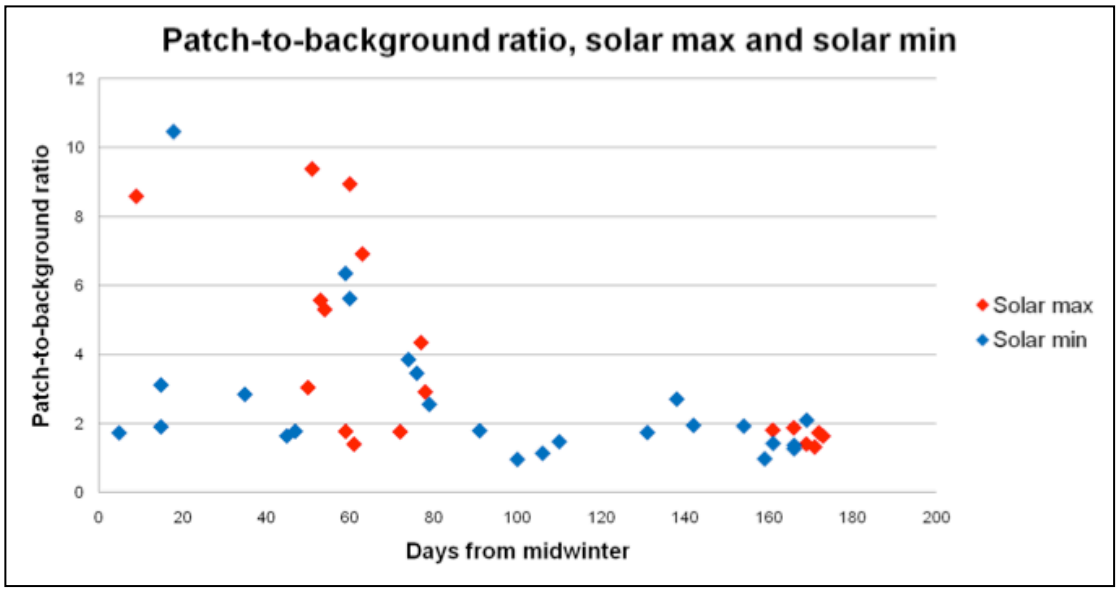

Relatively little variation between solar maximum & solar minimum

Enhancements weaker in summer

PLASLIFE: A code to calculate plasma decay rates

Simulation	Patch-to-Nightside Ratio
21 Dec	3.0 ± 0.9
21 Dec, thermospheric composition from 21 Jun	1.4 ± 0.4
21 Dec, initial plasma density from 21 Jun	1.7 ± 0.5
21 Dec, background plasma density from 21 Jun	2.3 ± 0.7
21 Dec, solar zenith angle from 21 Jun	3.0 ± 0.9
21 Dec, ion temperatures from 21 Jun	2.9 ± 0.9
21 Dec, neutral temperatures from 21 Jun	2.8 ± 0.9
21 Dec, optical depth from 21 Jun	2.7 ± 0.9
21 Jun	1.1 ± 0.4

Change was primarily due to variation in the chemical composition of the atmosphere. Maintenance of the background ionosphere by photoionisation in summer was a secondary effect (Wood and Pryse, 2010).

Statistical Study

Generalised Linear Modelling: (1192 observations)

Dependant Variable:

- Amount of plasma structuring

Independent Variables:

- Solar activity (F10.7 Solar Flux & SSN)
- Solar wind (IMF: Bx, By & Bz)
- Geomagnetic activity (Kp, AE)
- Plasma convection (Polar cap index)
- Season (days from midwinter)

Modelling Method

- Test statistical significance of all parameters
- Find the relative importance of the independent variables and which combination best represents the data

Svalbard

Parameter	Importance
Season	5.0
F10.7	3.5
Dst (average)	3.4
PCI (average)	2.9
SSN	2.9
Kp (average)	2.8
IMF Bz (average)	1.7
IMF Bz (stdev)	1.6
IMF By (stdev)	1.4
PCI (stdev)	1.3
AE (stdev)	1.2
Dst (stdev)	1.2
AE (average)	1.0
IMF Bx (stdev)	0.7
IMF Bx (average)	0.4
Kp (stdev)	0.1
IMF By (average)	0.0

Importance

Significance better than …

… 5% Importance 1

… 1% Importance 2

… 0.1% Importance 3

… 0.01% Importance 4

… 0.001% Importance 5

Season is the most important parameter

Results differ with:

- Location
- Altitude range
- Scale size of structure
- Time of day

Model Results

$$\log(STR) = \frac{1}{1.28 \cdot Season - 0.09 \cdot IMF\_Bz\_Stdev + 2.36}$$

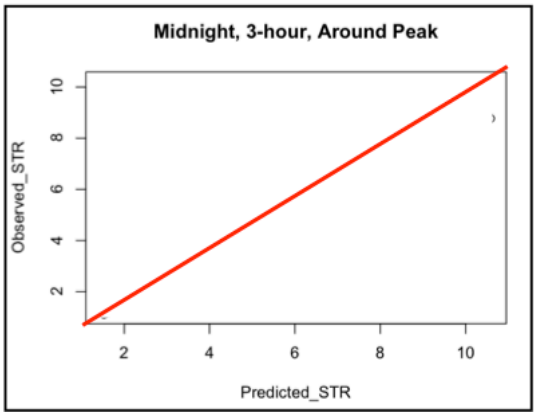

Need to include the effect of the neutral atmosphere

Testing a forecast: Goodness of fit statistics & skill scores; see review by Morley et al., (2018)

Beat climatology?

Useful Links

Extreme space weather: impacts on engineered systems and infrastructure, Royal Academy of Engineering (UK), 2013. https://www.raeng.org.uk/publications/reports/space-weather-full-report

Hapgood, M. (2017), Satellite navigation—Amazing technology but insidious risk: Why everyone needs to understand space weather, Space Weather, 15, 545–548, doi:10.1002/2017SW001638.
https://agupubs.onlinelibrary.wiley.com/doi/abs/10.1002/2017SW001638

Further Reading

Brekke, A., Physics of the Upper Polar Atmosphere, Wiley-Praxis Series in Atmospheric Physics, 1997.

Cannon, P. S. (2013), *Space Weather,* 11, 138-139, doi: 10.1002/swe.20032.

Crowley, G., Critical Review of patches and blobs, in Polar Cap Boundary Phenomena, in: URSI Review of Radio Science 1993-1996, edited by Stone, W. R., published for the International Union of Radio Science, Oxford University Press, 619-648, 1996.

Elmas, Z., et al. (2011), URSI General Assembly and Scientific Symposium, doi 10.1109/URSIGASS.2011.6123719.

Hapgood, M. (2017), Space Weather, 15, 545–548, doi:10.1002/2017SW001638.

Hargreaves, J. K., The solar-terrestrial environment, Cambridge atmospheric and space science series, Cambridge University Press, 1992.

Kinrade, J., et al. (2013), J. Geophys. Res., 118, doi: 10.1002/jgra.50214.

Kivelson, M. and C. Russell, Introduction to Space Physics, Cambridge University Press, 1996.

Morley, S. K., Brito, T. V., and Welling, D. T. (2018). Measures of Model Performance Based on the Log Accuracy Ratio, *Space Weather*, **16**, 69-88, doi:10.1002/2017SW001669

Mitchell, C. N. et al. (2005), Geophys. Res. Lett., 32, L12S03, doi:10.1029/2004GL021644.

Pryse, S. E., Wood, A. G., Middleton, H. R., McCrea, I. W., and Lester, M., Reconfiguration of polar-cap plasma in the magnetic midnight sector, Ann. Geophys., 24, doi:10.5194/angeo-24-2201-2006, 2201-2208, 2006.

Smith et al. (2008), Space Weather, 6, S03D01, doi 10.1029/2007SW000349.

Spogli, L., et al. (2009), Ann. Geophys., 27, 3429–3437, doi:10.5194/angeo-27-3429-2009.

Ünal, İ., E. T. Şenalp, A. Yeşil, E. Tulunay, and Y. Tulunay (2011), Performance of IRI-based ionospheric critical frequency calculations with reference to forecasting, Radio Sci., 46, RS1004, doi:10.1029/2010RS004428.

Weber, E. J., J. A. Klobuchar, J. Buchau, H. C. Carlson Jr., R. C. Livingston, O. de la Beaujadiere, M. McCready, J. G. Moore and G. J. Bishop, Polar cap F layer patches: Structure and dynamics, J. Geophys. Res., 91, 12121-12129, 1986.

Wood, A. G. and Pryse, S. E., Seasonal influence on polar cap patches in the high-latitude nightside ionosphere, J. Geophys. Res., 115, A07311, doi:10.1029/2009JA014985, 2010.

Wood, A. G., Pryse, S. E., Middleton, H. R., and Howells, V. S. C., Multi-instrument observations of nightside plasma patches under conditions of IMF B_z positive, Ann. Geophys., 26, 2203-2216, doi:10.5194/angeo-26-2203-2008, 2008.